



Modeling of the thermally induced residual stresses during laser transmission welding of thermoplastics

Christian Hopmann¹ · Simon Bölle¹ · Suveni Kreimeier¹

Received: 15 November 2018 / Accepted: 3 July 2019 / Published online: 20 July 2019
© International Institute of Welding 2019

Abstract

Laser transmission welding is one of the various welding techniques used to join thermoplastics. Low heat introduction into the welded parts and a high welding speed are the reasons why laser transmission welding established itself in the plastic processing industry. In all welding processes for thermoplastics, residual stresses occur due to the thermal expansion during heating and its resetting during subsequent cooling. These thermally induced residual stresses impair the mechanical properties of the welded components. To estimate the residual stresses and therefore to improve the process setup and understanding of the welding process, a thermo-mechanical simulation model for the laser transmission welding is developed at the IKV. In a linked simulation, the temperature distribution and mechanical stresses are calculated parallelly for each time step. The material, a polyamide 6.6, is modeled with elastic, elastoplastic, and linear viscoelastic behavior. After cooling, residual stresses of a realistic magnitude are calculated. However, as the yield point of the polyamide is exceeded in the welding process, the tensile/compression ratio in the welded component is only mapped correctly for the elastic-plastic material model.

Keywords Heat-affected zone · Laser transmission welding · Residual stresses · Simulation · Temperature distribution

1 Introduction

Due to their versatile properties and continuous development, plastics are found in a wide range of consumer and industrial applications [9, 40, 48]. Plastic products are also increasingly used in areas with high requirements such as electrical, automotive, or aerospace technology and this leads to increasing demands on the manufacturing process [22, 28]. The joining process is usually one of the last steps in the manufacturing process and often determines the functionality of a component [4, 35].

An industrially established joining process is the laser transmission welding of plastics, in which a laser-transparent welding partner and a laser-absorbing welding partner are joined together in a material-locking manner [9, 23, 45]. Since the weld is often a weak point and thus a potential

failure point in the component, the weld strength is required for the mechanical design of laser-welded components. In addition to the basic strength of the welded materials, this is largely dependent on the welding process and cannot be estimated with sufficient accuracy on the basis of the process parameters used. Welded components are therefore designed in an iterative process in which both the welding parameters and the actual geometry of the welding zone are adapted in accordance with guidelines. In order to significantly reduce the design effort and to extend the understanding of the process, a multi-scale simulation for the numerical description of the welding strength of welded components is to be developed using laser transmission welding as an example (Fig. 1).

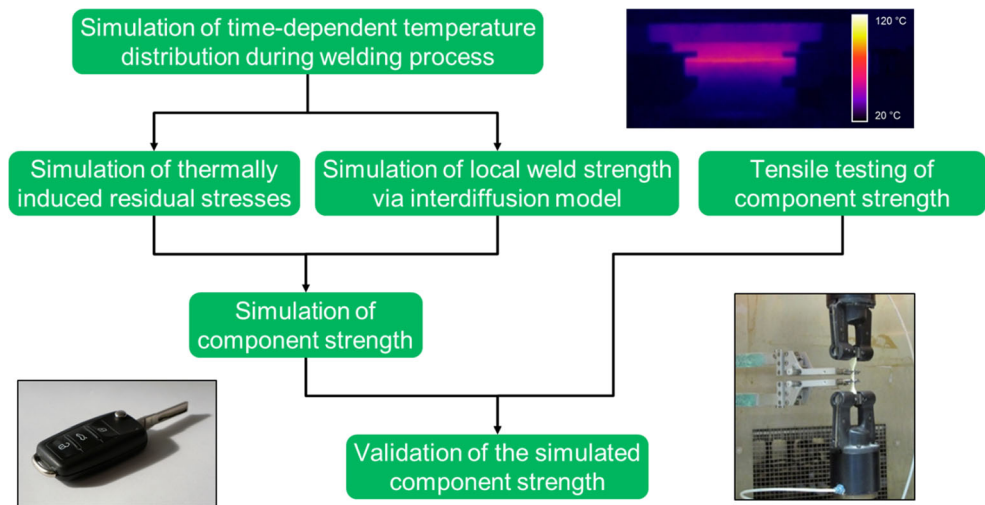
In the first step, a three-dimensional model for the thermal description of the laser transmission welding process is developed. This provides the time-dependent and spatial temperature field in the welding zone, which forms the basis for further calculations. The strength distribution in the welding zone can be described by simulating the interdiffusion processes on the molecular level on the basis of the reptation model of de Gennes [10]. The welding zone strength is initially a local mechanical parameter. However, the strength of a weld in a component or assembly is also influenced by the residual stresses in the welding zone induced thermally during the

Recommended for publication by Commission XVI - Polymer Joining and Adhesive Technology

✉ Simon Bölle
Simon.Boelle@ikv.rwth-aachen.de

¹ Institute of Plastics Processing (IKV), RWTH Aachen University, Aachen, Germany

Fig. 1 Concept for the numerical description of the weld strength in welded components



welding process. Based on the thermal calculations, a thermomechanical model for determining the residual stress distribution in the weld seam as a function of the welding parameters is therefore to be developed. A simulative determination of both the strength and the residual stress distribution makes it possible to map the structural behavior of welded components.

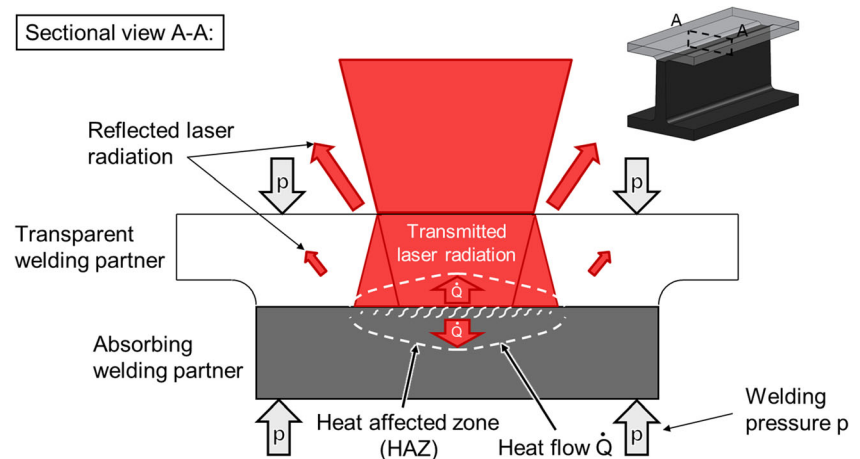
2 Laser transmission welding

In laser transmission welding, two welding partners are positioned one on top of the other without gaps using a welding device and a welding pressure p is applied. The process principle is shown in Fig. 2. Ideally, the laser beam passes through the laser-transparent welding partner facing the focusing optics without loss and is absorbed close to the surface by the laser-absorbing welding partner facing away. The laser-transparent welding partner is then also heated by heat conduction, so that both welding partners

are plasticized. Due to interdiffusion processes in the heat-affected zone (HAZ), the welding partners are joined together under the external and internal welding pressures resulting from the expansion of the melt [8, 37, 41, 52].

Influences on the weld seam quality are the laser source used, the process control, and the properties of the molded part (design boundary conditions) or the material used. On the material side, the optical and thermal properties are decisive. The optical properties are the transmittance, reflectance, and absorption coefficient for the laser radiation used and the transmission behavior in the material (change in the laser intensity distribution). Thermal material properties include specific heat capacity, thermal conductivity, and density. In the process settings, laser power, irradiation time, welding pressure, power density distribution of the laser radiation, and the process variant used are relevant influencing variables on the weld seam quality. This is assessed on the basis of the strength and uniformity of the seam width, tightness, reproducibility, and HAZ [23, 28, 29].

Fig. 2 Process principle of laser transmission welding



Since the mid-1990s, various research institutions have been presenting approaches for the analytical calculation of the temperature distribution in the heating phase of laser transmission welding [24–27, 46]. The modeling is based on a number of simplifying factors regarding the material properties or the intensity distribution of the laser beam.

Furthermore, different approaches for the numerical calculation of the heating process using the finite element method (FEM) are pursued [1, 3, 5, 7, 11–13, 15, 21, 26, 32–34, 50, 54]. As a numerical approximation method, the FEM makes it possible to model the welding partners from small (finite) elements [49]. This makes it possible to observe more complex and three-dimensional geometries, in which analytical methods quickly reach their limits [49]. The listed works differ in the type of modeling as well as in the input parameters used. Both literature values and own measurements serve as input data, whereby the measuring methods used vary. Challenges arise with the temperature dependence of the material properties, the characterization of the intensity distribution, the experimental validation of the calculated temperature distributions, and the deviations between simulation results and experimentally determined results.

Potente et al., Zoubair and Elhem, and Gupta and Pal present first results for thermomechanical calculations of contour welding [18, 43, 54]. Potente et al. calculate temperatures up to 250 °C and, after cooling, tensile residual stresses in the transmission direction up to 25 MPa using an elastic-viscoplastic material model for polycarbonate (PC). However, it seems questionable that the calculated tensile stresses after cooling decrease with lower scanning speed of the laser and thus higher temperatures in the welding process. Zoubair and Elhem calculate temperatures up to 700 °C, which appear very high. The temperatures result in residual stresses up to 30 MPa using an elastoplastic material model for polypropylene (PP). Since the von Mises equivalent stress is considered, it is not possible to make any statements about the tensile/compression ratios. Zoubair and Elhem calculate temperatures up to 700 °C, which appear very high. The temperatures result in residual stresses up to 30 MPa using an elastoplastic material model for polypropylene (PP). Gupta and Pal calculate temperatures of up to 480 °C that result in residual tensile stresses up to 2 MPa in the scanning direction. Information on the mechanical material model for the polyamide 6 (PA 6) under consideration was not provided and residual stresses in other directions were not considered. Labeas et al. present a simulation model for the calculation of residual stresses during contour welding of composite parts [31]. Temperatures of 320 °C are calculated, which lead to residual stresses of 14 MPa. In the calculation, however, simple, purely elastic material behavior is assumed for both components of the composite. Furthermore, all previous work on thermomechanical simulation has in common that no detailed validation of the simulation results has taken place.

The aim of the subsequent investigation is therefore the realistic numerical description of the temperature distribution in the welding zone and the thermally induced residual stresses in the simultaneous welding process as a function of the welding process parameters. For this purpose, temperature-dependent material models for elastic, elastoplastic, and viscoelastic mechanical behavior are considered and evaluated.

3 Thermal simulation

3.1 Simulation model for simultaneous welding

In the presented study, the process variant of simultaneous welding for a polyamide 66 (PA 66) of the type Ultramid A3W of the manufacturer BASF SE, Ludwigshafen, Germany, with 0.3 wt.% carbon black at the laser-absorbing welding partner is considered. Two T-shaped test specimens are welded as shown in Fig. 2. In the simultaneous welding process, the entire seam contour is joined at the same time with one or more laser sources. In this investigation, the process parameters laser power and irradiation time are varied. The FEM program Abaqus from Dassault Systèmes SE, Vélizy-Villacoublay, France, is used for the simulation.

Laser transmission welding is modeled as a 3D heat conduction problem using the Fourier differential equation [28, 42]. The Fourier differential equation is shown in Eq. 1 [6]:

$$\frac{\partial E}{\partial t} + \vec{v} * \nabla E = \nabla(\lambda \cdot \nabla T) + \dot{Q}''' \quad (1)$$

With $\frac{\partial E}{\partial t} = \frac{\partial}{\partial t} (\rho(T) \cdot c_p(T) \cdot T(t))$ (change of the internal energy)

$\vec{v} * \nabla E$ (convective energy flux)

$\nabla(\lambda \cdot \nabla T)$ (diffuse energy flux/heat conduction)

\dot{Q}''' (absorbed volume heat flux)

E corresponds to energy in [J], t to the time in [s], \vec{v} to the flow velocity in [m/s], λ to the thermal conductivity in [W/(m·K)], T to the temperature in [K], \dot{Q}''' to the absorbed volume heat flux in [J/(s·m³)], ρ to the density in [kg/m³], and c_p to the specific heat capacity in [J/(kg·K)]. Since for the specimens used there is only a minimal melt flow in the direction of the weld seam in experimental welds, no melt flow is implemented in the simulation to simplify matters. Equation 2 results without the convective energy flux [28]:

$$\frac{\partial}{\partial t} (\rho(T) \cdot c_p(T) \cdot T(t)) = \nabla(\lambda \cdot \nabla T) + \dot{Q}''' \quad (2)$$

\dot{Q}''' represents the volume heat flux applied by the laser radiation and is implemented in Abaqus via a Fortran

subroutine. The calculation of the volume heat flux is shown for the transparent welding partner in Eqs. 3–6:

$$\dot{Q}''' = \frac{dQ'''}{dt} \tag{3}$$

$$q''' = \frac{dQ'''}{dV(\rho, T)} \tag{4}$$

$$q''' = I_T(x, z) \cdot \frac{d}{dy} \alpha_T(y) \tag{5}$$

$$\begin{aligned} \frac{d}{dy} \alpha_T(y) &= \frac{d}{dy} [(1-R_T) \cdot (1-e^{-\varepsilon \cdot y})] \\ &= (1-R_T) \cdot e^{-\varepsilon \cdot y} \cdot \varepsilon \end{aligned} \tag{6}$$

Q corresponds to the heat in [J], t to the time in [s], q''' to the heat per volume [J/m³], V to the volume in [m³], I_T to the intensity distribution of the laser when hitting the transparent joining partner in [W/m²], R_T to the unitless reflection factor, and ε to the extinction coefficient in [m⁻¹]. The location is determined by the path coordinates x , y , and z in [m]. With Eqs. 3 and 4 assumed, the calculation of the volume heat flux for the absorbing welding partner is carried out according to Eqs. 7 and 8:

$$q''' = I_A(x, z, \varepsilon, \rho_A) \cdot \frac{d}{dy} \alpha_A(y) \tag{7}$$

$$\frac{d}{dy} \alpha_A(y) = \frac{d}{dy} [1 - e^{-\alpha \cdot (y-d)}] = \alpha \cdot e^{-\alpha \cdot (y-d)} \tag{8}$$

ρ_A corresponds to the unitless surface reflection at the absorbing welding partner and α to the absorption coefficient in [m⁻¹]. Altogether, the input parameters for the model are the thermal material properties (thermal conductivity λ , density ρ , specific heat capacity c_p), the optical properties (absorption coefficient α , extinction coefficient ε , surface reflection ρ_A , reflection factor R_T) and the properties of the laser intensity profile $I_T(x, z)$, and the intensity profile of the transmitted laser radiation $I_A(x, z, \varepsilon, \rho_A, R_T)$.

In order to limit the complexity of the simulation, the temperature dependence of the optical material properties, the thermal radiation emitted by the component to the environment, and an anisotropy of the materials are not taken into account. Furthermore, an ideal heat transfer is assumed between the two welding partners, which is achieved by a very high heat transfer coefficient of 10⁹ W/(m² × K). It is thus presupposed that the heat flow at the contact surface between the two welding partners is not attenuated.

3.2 Sensitivity analysis

The laser transmission welding process is subject to many influencing variables which, especially in the form of the input data in the preceding simulation models, lead to challenges

both in the determination and in the type of implementation [1, 3, 5, 7, 11–13, 21, 25, 34, 46, 54]. In order to test the influence of the different input data on the simulation results with a justifiable calculation effort, a sensitivity analysis for the simulation is carried out as a simplified 2D model by Kreimeier [28]. In the joining area, elements with a size of 10 × 10 μm² are used. In the sensitivity analysis, the thermal model is calibrated using literature data for the input parameters. The literature data obtained for the starting temperature of 23 °C are presented in Table 1. The density and the specific heat capacity are implemented temperature-dependently up to the melt range. Even if the thermal conductivity fluctuates for different temperatures, it is not possible to define an unambiguous course over the temperature due to the scattering of currently available measuring systems [28]. The thermal conductivity is therefore assumed to be constant. Furthermore, a change of the optical properties is to be expected in the melt range. However, currently available measurement methods only allow the optical properties to be determined at room temperature, which is why temperature-independent properties are also assumed here.

Calculations are performed by increasing the input parameters by 20% to determine which parameters the model is particularly sensitive to [53]. In this way, it is shown to what extent an exact determination of the input parameters is necessary. According to Eq. 2, the data considered are the specific heat capacity c_p , the thermal conductivity λ , the density ρ , and the volume heat flux \dot{Q}''' introduced. In the second step, the influence of the optical properties is analyzed as part of the subroutine for the volume heat flux. These are the absorption coefficient α , the extinction coefficient ε , the surface reflection at the absorbing welding partner ρ_A , and the reflection factor at the transparent welding partner R_T . Sensitivity analysis is performed with a laser power of $P_L = 50$ W and an irradiation time of $t_l = 0.75$ s for constant welding parameters. The target value is the size of the HAZ in [mm²], which is

Table 1 The literature data obtained for the starting temperature of 23 °C

Input parameter	Unit	Value	Reference
Thermal material properties			
Density, ρ ¹	kg/m ³	1155	[39]
Specific heat capacity, c_p ¹	J/(kg × K)	1591	[38]
Thermal conductivity, λ	W/(m × K)	0.33	[39]
Optical material properties			
Absorption coefficient, α	m ⁻¹	18.181	[46]
Extinction coefficient, ε	m ⁻¹	137.21	[2]
Surface reflection, ρ_A	–	0.0539	[44]
Reflection factor, R_T	–	0.61295	[2]

¹ Temperature-dependent modeling

approximated as an ellipse with width W in [mm] and height H in [mm] (Eq. 9). The results of the sensitivity study are shown in Figs. 3 and 4.

$$HAZ = \frac{\pi}{4} \cdot W \cdot H \tag{9}$$

It can be seen that the heat flux has the highest influence on the HAZ. The thermal properties describe how the energy of the heat flux is absorbed and distributed in the component. An increase in one of the thermal material properties always results in a reduction of the HAZ. The specific heat capacity describes the amount of energy required to increase the temperature. An increase in the heat capacity therefore means that a lower maximum temperature is reached with the same energy. This results in a smaller HAZ. The effect of thermal conductivity is also negative. Due to the increase in thermal conductivity, the heat in the material is dissipated more quickly in all directions. The energy required to melt the plastic is not available in the welding zone, so that less plastic is melted and a smaller HAZ is produced. The negative effect of density is directly related to the specific heat capacity, which is calculated per mass. An increase in density means that there is more mass in the same volume. This requires more energy to melt the volume and reduces the size of the HAZ. The interactions between the individual factors are minimal. The greatest interactions are between the heat flux and the specific heat capacity as well as the volume heat flux and the density. Since these factors have the greatest effect on the HAZ, the resulting interactions are also most pronounced.

Compared with the thermal material properties, the optical properties exhibit significantly less pronounced effects and interactions. Only the extinction coefficient shows a clear influence. This describes how much energy reaches the welding zone. An increase means that more energy is already absorbed

or reflected before the welding zone. Thus, the extinction coefficient has a negative influence on the HAZ. Since it can be assumed that the radiation reaching the absorbing welding partner is almost completely absorbed over a thickness of 2 mm, there is no major influence of the degree of absorption on the size of the HAZ. It is to be expected that a higher degree of absorption leads to a near-surface absorption and thus to a larger width and lower height of the HAZ. However, width and height were not considered separately in the sensitivity study. For the surface reflection of the absorbing welding partner, there is no clearly pronounced effect, since the reflected radiation has only a very small share compared with the absorbed radiation. The reflection factor of the transparent welding partner is only used for the transparent welding partner to calculate the volume heat flow applied by the laser (Eqs. 5 and 6). Since the significantly larger volume heat flux in the absorbing welding partner is calculated using the extinction coefficient (Eqs. 7 and 8), the reflection factor is not used here and thus does not show a clearly pronounced effect on the size of the HAZ.

3.3 Optimization of a three-dimensional simulation model

Based on the sensitivity analysis carried out, it can be deduced that a precise characterization of the input data is indispensable for a realistic simulation. The determination of the specific heat capacity, the thermal conductivity, and the density as well as the extinction coefficient in the transparent welding partner are of particular importance. For the development of a three-dimensional model, the input data for the material used are determined experimentally. To determine the density and the thermal conductivity as a function of temperature, the pvT measuring device pvT100 from SWO Polymer-technik

Fig. 3 Effects and interactions on the change of HAZ in the sensitivity analysis (thermal material properties) [28]

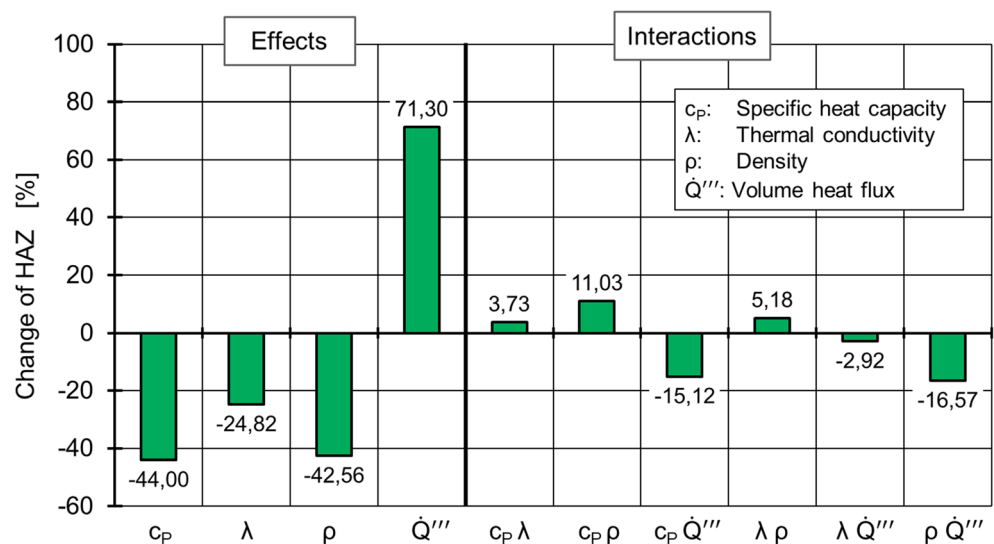
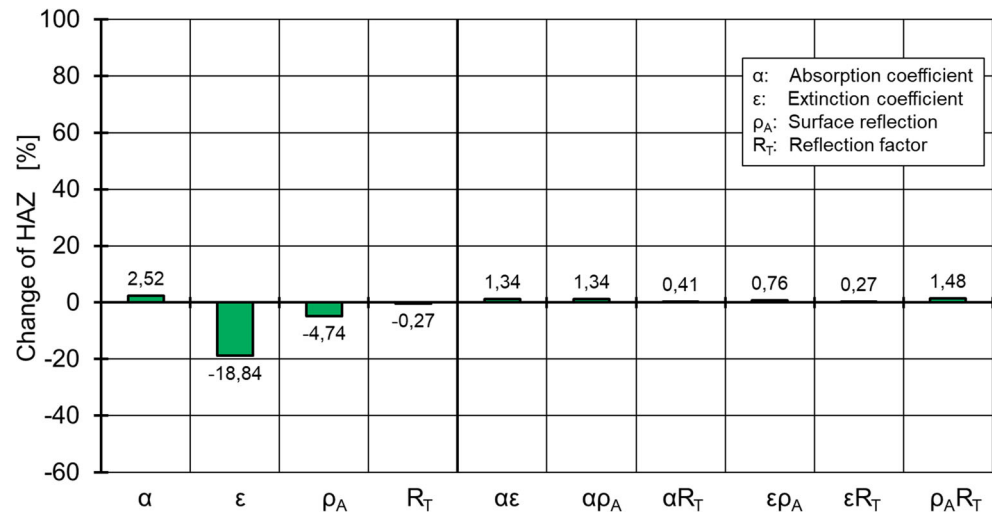


Fig. 4 Effects and interactions on the change of HAZ in the sensitivity analysis (optical material properties) [28]



GmbH, Krefeld, Germany, is used. The temperature-dependent specific heat capacity is determined using a differential scanning calorimetry device of the type DSC Q2000 from TA Instruments Inc., New Castle, USA. The optical properties are determined using a Lambda 1050 spectrometer from PerkinElmer Inc., Waltham, USA. The experimentally determined input data compared with the literature data from Section 3.2 are shown in Table 2.

Both for the literature-based simulation and for the simulation based on the experimentally determined input data, the accuracy is checked for various welding process points. The experimental welding tests are carried out with a fiber-coupled diode laser of type LDM 400-40 from Laserline GmbH, Mühlheim-Kärlich, Germany, with a wavelength of 940 nm and a linear focus of $27 \times 1.5 \text{ mm}^2$. For validation, the HAZ is determined using a DM 4000M transmitted light microscope from Leica Microsystem GmbH, Wetzlar, Germany. The results are shown in Fig. 5.

As expected, a higher energy input in the form of increased laser power P_L or irradiation time t_l leads to increased HAZ

both in experimental welds and in the simulations. It can be seen that the simulation with experimentally determined input data for all considered combinations of laser power and irradiation time leads to calculated HAZ that is closer to the HAZ of experimental welds. Nevertheless, the HAZ is clearly overestimated in both simulations.

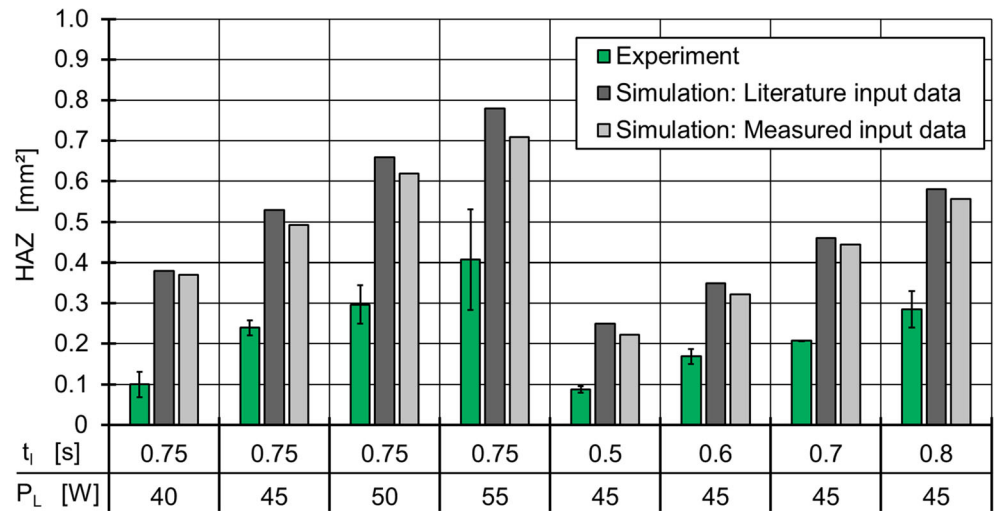
The reason for this is the determination of the extinction coefficient ϵ using the Lambda 1050 spectrometer. For the measurement, a measuring beam with parallel directed, monochromatic light with a wavelength of 940 nm is generated via various lamps, monochromators, and mirrors. An Ulbricht sphere integrated in the instrument serves as the measuring unit. The schematic structure of the measuring system is shown in the left of Fig. 6. Next to an opening for the reference measuring beam, there is a measuring port on which a plate-shaped specimen of 2-mm thickness is positioned. The diffusing and highly reflective BaSO4 coating of the inner sphere surface distributes all incident light through the ports, both directional and diffuse radiation, evenly over the surface. Photodetectors locally detect the photovoltage induced by

Table 2 The experimentally determined input data compared with the literature data

Input parameter	Unit	Value (literature)	Value transp. (measured)	Value abs. (measured)
Thermal material properties				
Density, ρ^1	kg/m ³	1155	1124	1133
Specific heat capacity, c_p^1	J/(kg × K)	1591	1815	1701
Thermal conductivity, λ	W/(m × K)	0.33	0.284	0.266
Optical material properties				
Absorption coefficient, α	m ⁻¹	18.181		21.43
Extinction coefficient, ϵ	m ⁻¹	137.21	140.92	
Surface reflection, ρ_A	%	5.39		5.39
Reflection factor, R_T	%	61.295	79.157	

¹ Temperature-dependent modeling

Fig. 5 Comparison of the HAZ areas from the simulations with experimental welds



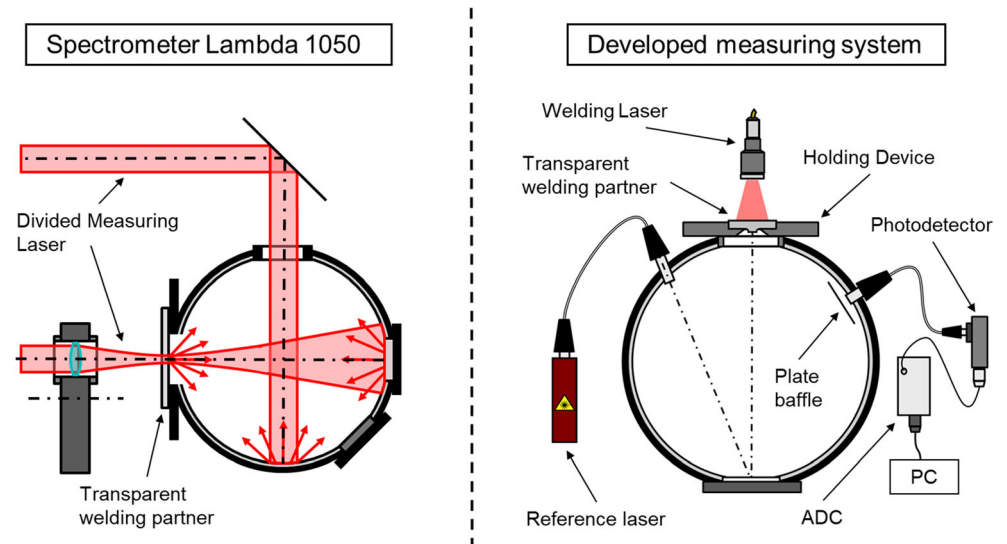
the intensity prevailing on the surface of the sphere, allowing conclusions to be drawn about the total irradiated power. For the measurement, a calibration is first carried out in which the measuring beam is directed into the Ulbricht sphere without interaction with the specimen and the photovoltage present at the detectors is measured. The voltage is determined as a reference for a transmittance of $\tau = 1$. The reference value for $\tau = 0$ is determined by a measurement with the measuring beam switched off. By interpolation between the two values, the intensity recorded during the measurement of the specimen is converted into the transmittance. In addition, reference measurements are carried out during the actual measurement. For this purpose, the measuring beam is alternately directed into the Ulbricht sphere via a mirror segment chopper via the primary port and the reference port. With this additional measurement, errors resulting from surface defects are

mathematically corrected. From the determined degree of transmittance τ at a thickness d of the test specimen, the extinction coefficient ϵ can be calculated according to Eq. 10:

$$\epsilon = -\frac{\ln(\tau(d))}{d} \tag{10}$$

A problem with the transmission measurement with the spectrometer is the deviating focus of the measuring beam from the line optic used for the laser source in the welding process. On the other hand, the measuring beam is scattered and expanded, especially when semicrystalline materials are used, so that some of the radiation does not reach the measuring opening of the Ulbricht sphere. The opening thus functions as an aperture, which reduces the transmitted measuring beam by an unknown proportion

Fig. 6 Measuring systems for the extinction coefficient



depending on the specimen and measuring beam. This proportion cannot be determined or corrected exactly and is included in the determined performance as a systematic error. Since the measurement of the transmittance by spectrometer does not allow an exact determination of the intensity distribution, a measuring stand is developed with which the power is measured directly after leaving the transparent welding partner. For this purpose, a measuring system based on an Ulbricht sphere is set up under the focusing optics of the welding laser (Fig. 6, right). The transparent welding partners are placed in a holding device on the Ulbricht sphere. The holding device acts as an aperture that only permits radiation transmission into the Ulbricht sphere through the focused $27 \times 1.5 \text{ mm}^2$ welding surface of the transparent welding partners. The welding laser is focused on the underside of the specimen in order to depict the welding process as realistically as possible. In this way, the power introduced into the welding zone can be determined directly. The determined degrees of transmission and resulting extinction coefficients are shown in Table 3.

It is shown that the transmission into the transparent welding partner is overestimated in the spectrometer measurement, which explains the deviation of the simulation results from experimental welds (Fig. 5). The simulation with the newly determined transmittance leads to calculated HAZ for all considered laser powers and irradiation times, which are to be classified as very realistic (Figs. 7 and 8).

4 Thermomechanical simulation

For thermomechanical simulation, the thermal simulation model described in Section 3 is coupled with a mechanical simulation to calculate the residual stresses induced in the welding process. In the coupled simulation, the temperature distribution and the mechanical load are calculated in parallel for each time step. The calculation is based on the thermal expansion ε of the material and its resetting due to the temperature gradients in the two welding partners during heating and cooling in the welding process. The strain is calculated using Eq. 11 [16].

$$\varepsilon = \alpha \cdot (T - T_0) \quad (11)$$

Table 3 The determined degrees of transmission and resulting extinction coefficients

	Spectrometer Lambda 1050	Developed measuring system
Degree of transmission, τ	0.7544	0.6146
Extinction coefficient, ε	140.92	243.38

The thermal expansion coefficient α is measured as a function of temperature using the thermal-mechanical analysis device TMA 2940 from TA Instruments. The calculation of the residual stresses from the thermally induced stresses is initially based on three different temperature-dependent material models. These are an elastic (Eq. 12, [16]), an elastoplastic (Eq. 13, [14]), and a viscoelastic material model (Eqs. 14 and 15, [20, 30, 36, 47]). The mechanical properties of the material are assumed to be isotropic in the simulation model.

$$\sigma = E \cdot \varepsilon \quad (12)$$

$$\sigma = E \cdot \varepsilon_{el} + \sigma_{pl} \quad (13)$$

$$\sigma(t) = E(t) \cdot \varepsilon(t) \quad (14)$$

$$E(t) = E_{\infty} + \sum_{i=1}^n E_i \cdot e^{-\frac{t}{\tau_i}} \quad (15)$$

To determine the temperature-dependent mechanical characteristics for the thermomechanical calculation, the universal testing machine type Z150 of Zwick GmbH & Co. Kg, Ulm, Germany, is used in combination with the temperature chamber type KEE250/75K from RS Simulatoren Prüf- und Messtechnik GmbH, Oberhausen, Germany. The parameters required for the elastic and elastoplastic material model can be derived from the stress-strain curves determined in the tempered tensile tests and implemented in the model.

The viscoelastic material model is able to describe the effects caused by creep or relaxation, i.e., the time-dependent mechanical behavior of the material. Küsters developed a method for the determination of viscoelastic properties by strain-controlled short-term tensile tests [30]. A scheme of the procedure is shown in Fig. 9.

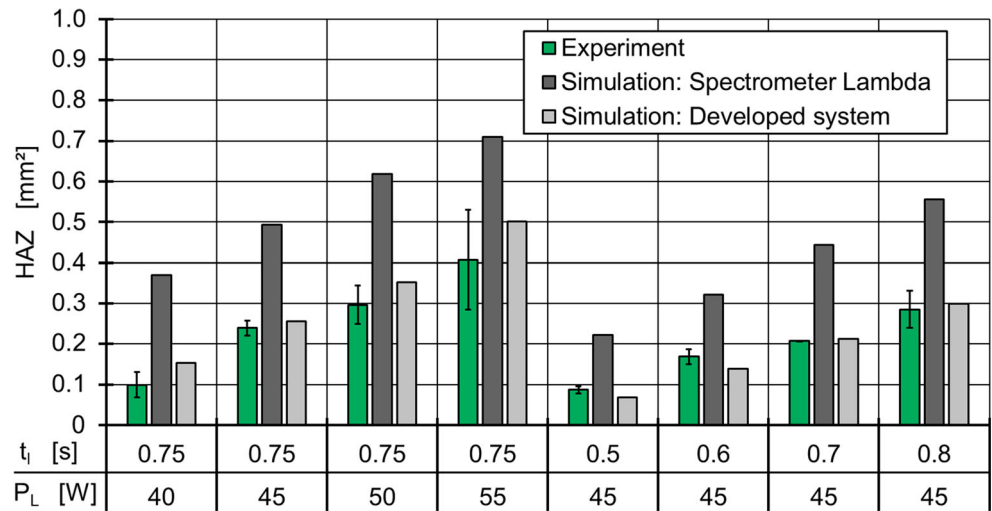
Due to low elongation in the welding process, linear viscoelasticity is assumed and a 2-parameter approach is used. The equation of the 2-parameter approach is:

$$\sigma(\varepsilon) = E_0 \cdot \varepsilon_{\tau} \left(1 - e^{-\frac{\varepsilon}{\varepsilon_{\tau}}}\right) \quad (16)$$

Here, E_0 is the origin modulus of elasticity and ε_{τ} is the relaxation strain. In the stress-strain diagram, relaxation strain describes the strain at which the straight line of E_0 intersects the line of the maximum component stress. Since this calculation must be repeated for each temperature and strain rate, a Microsoft Excel macro was developed as part of Küsters' dissertation, which automatically determines these parameters. Subsequently, the parameters can be shifted over a large time range using the time-temperature shift principle and combined to form a master curve.

A Prony fit is performed for both parameters to generate a young modulus master curve. The Prony-Fit models viscoelastic material behavior by means of a parallel connection of several spring/damper elements. With a sufficient number of row links, the material behavior can be realistically

Fig. 7 Comparison of the HAZ areas from the simulations with different extinction coefficients with experimental welds



mapped. The model is called the generalized Maxwell model [51]. The relaxation modulus based on the Prony series is calculated according to Eq. 14. For the determination of the Prony parameters, tensile tests with each combination of the strain rates 10, 100, 1,000, and 10,000%/h and the temperatures $-20, 0,$ and $20\text{ }^\circ\text{C}$ are performed. For the Prony-Fit, six row links are determined for the range from 10^{-5} to 10^1 s, and the resulting master curve is implemented in the material model.

Figure 10 shows the signed von Mises stress over time during heating and cooling in the laser welding process. For the marked finite element, the curves for the three material models with a laser power P_L of 70 W and an irradiation time t_I of 0.5 s are displayed. In order to reduce the calculation

times, the two axes of symmetry of the test specimens are used in the simulation. The marked element is therefore the element which lies exactly in the middle of the weld and thus reaches the highest temperatures. Looking at the signed von Mises stress, it becomes clear that increasing compressive stresses are initially formed in the simulation during heating due to the thermal expansion with increasing temperature. During the subsequent cooling process, these form back completely for the elastic and viscoelastic material model. Significant differences between elastic and viscoelastic material models do not form during the cooling process. Only the elastoplastic material model is capable of mapping the plastic strain components resulting from exceeding the yield point. These prevent a complete resetting of the material and thus result in the

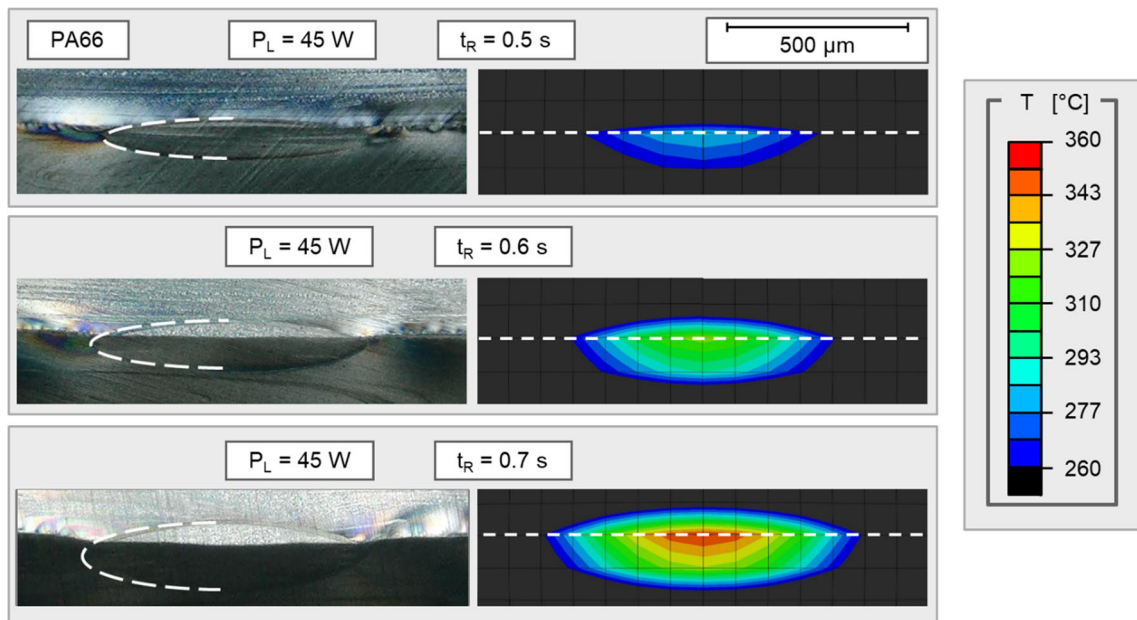
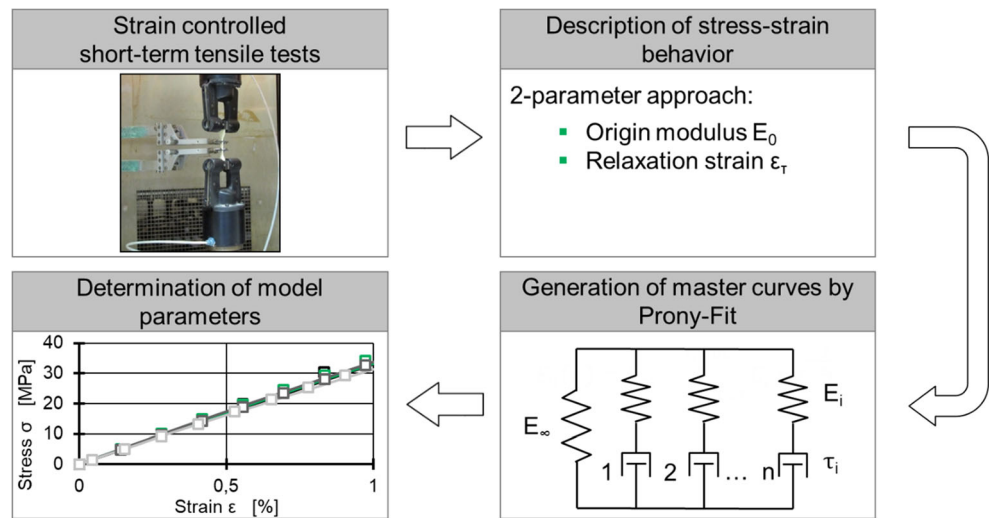


Fig. 8 Validation of the thermal simulation model based on the optical appearance of the HAZ

Fig. 9 Calibration of a linear viscoelastic material model according to Küsters [30]



expected tensile stresses in the weld during cooling. The fluctuations of the residual stresses in the range of the cooling time between 2 and 4 s are caused by the time-shifted sign changes of the main stresses σ_x and σ_z , which the signed von Mises stress cannot meaningfully represent (Fig. 11). However, the curves of the individual main stresses are continuous. Overall, only the elastoplastic material model leads to a realistic tensile compression ratio during the welding process. Therefore, only the elastoplastic material model is considered in the further investigations.

Figure 12 shows the fitted signed von Mises stress in the finite element described above for different process parameters. For the purpose of clarity, a constant irradiation time t_f of 0.5 s is observed, at which the laser power P_L is varied between 50 W, 70 W, and 90 W. A higher laser line, i.e., a stronger heating in the welding process, leads to a higher thermal expansion in the heating process

and thus to higher compressive stresses in the finite element under consideration. The greater thermal expansion in conjunction with higher temperature gradients in the cooling process in turn cause the formation of larger plastic expansion components, which result in greater tensile stresses after cooling.

In addition to the stress curve in the middle element, Fig. 12 shows the spatial stress distributions for the welding process after 0.5 s (after heating), 1 s, 10 s, and 20 s (after cooling). The spatial signed von Mises stresses in the drawn x -direction after heating and after cooling are shown in more detail in Fig. 13. After heating, compressive stresses are calculated in the area of the weld and the immediate environment due to the thermal expansion. The maximum compressive stress is exactly centered in the weld ($x = 2$ mm). For mechanical compensation, tensile stresses are created at the edges of the model. After cooling, the expected tensile stresses form in the weld

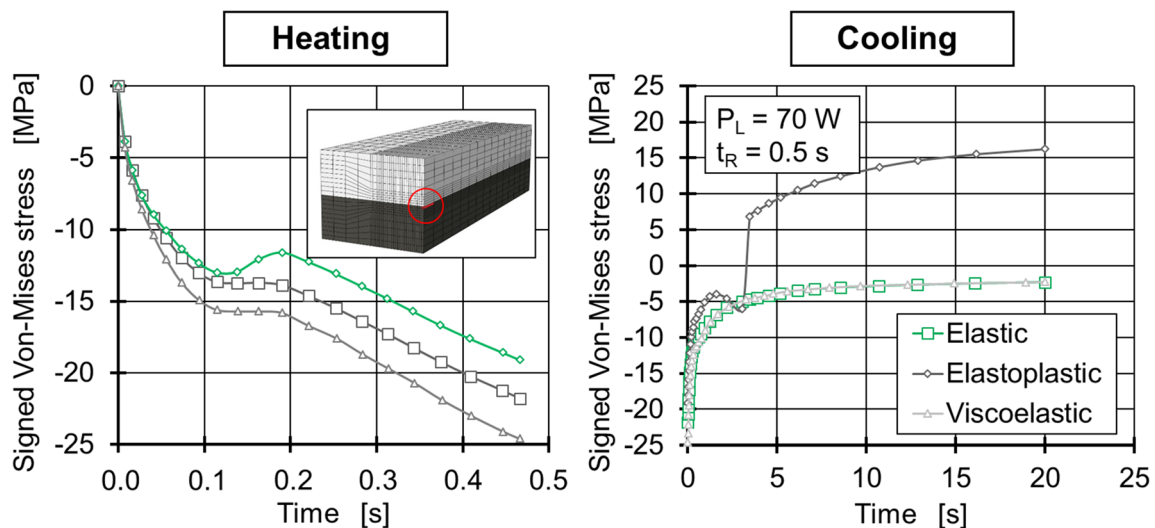


Fig. 10 Signed von Mises stresses during the welding process for the three material models

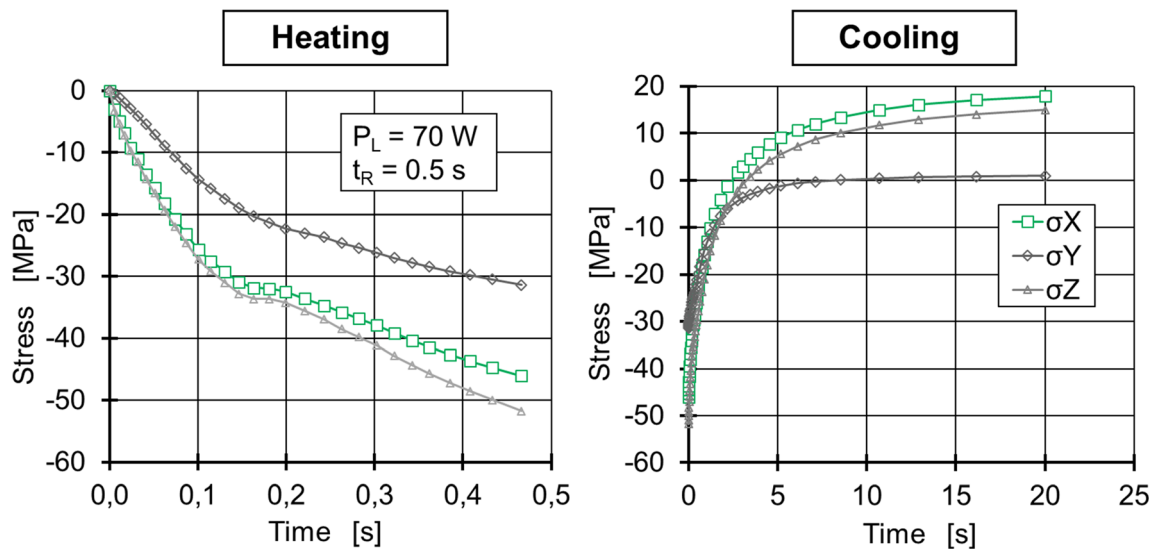


Fig. 11 Main stresses during the welding process in the three directions for the elastoplastic material model

seam in reverse, which are in mechanical equilibrium with the compressive stresses in the vicinity of the weld. As expected, the maximum tensile stress is again in the center of the weld. As with the temporal course of stresses in the central finite element, an increase in tensile and compressive stresses also occurs spatially with an increase in laser power.

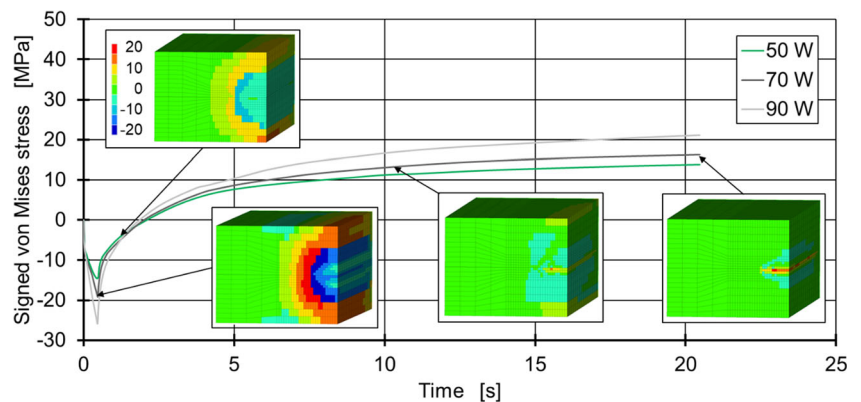
The conventional method for the quantitative determination of internal stresses is the hole drilling method, with which, however, only residual stresses up to a material depth of 0.6–0.8 mm can be measured validly. A quantitative validation of the calculated residual stresses in the weld at a depth of 2 mm is therefore not possible with current methods. However, since residual stresses in the injection molding process are in the range of 5–10 MPa [17, 19] and significantly higher temperature gradients are present in the laser welding process, it can be assumed that the calculated results are in a realistic order of magnitude. In addition, the tensile-compression ratios are mapped correctly in the simulation.

5 Conclusion and outlook

In the presented study, a sensitivity study was performed on a 2D thermal simulation model calibrated with literature data. By targeted variation of the input parameters, the thermal material properties density, thermal conductivity, and specific heat capacity as well as the extinction coefficient of the laser-transparent welding partner were identified as particularly influencing on the heat-affected zone in the simulated laser welding process. Through a precise experimental determination of the thermal properties and a newly developed measuring setup for the determination of the extinction coefficient, a 3D model could be developed, which leads to realistic calculation results for the HAZ.

Based on the thermal 3D model, a thermomechanical model with elastic, elastoplastic, and viscoelastic material behavior was then developed. Only the elastic-plastic material model leads to a realistic calculation of the tensile-compression ratios of thermally induced residual stresses during the welding

Fig. 12 Fitted signed von Mises stresses over time for the elastoplastic material model with laser powers of 50 W, 70 W, and 90 W and a radiation time of 0.5 s



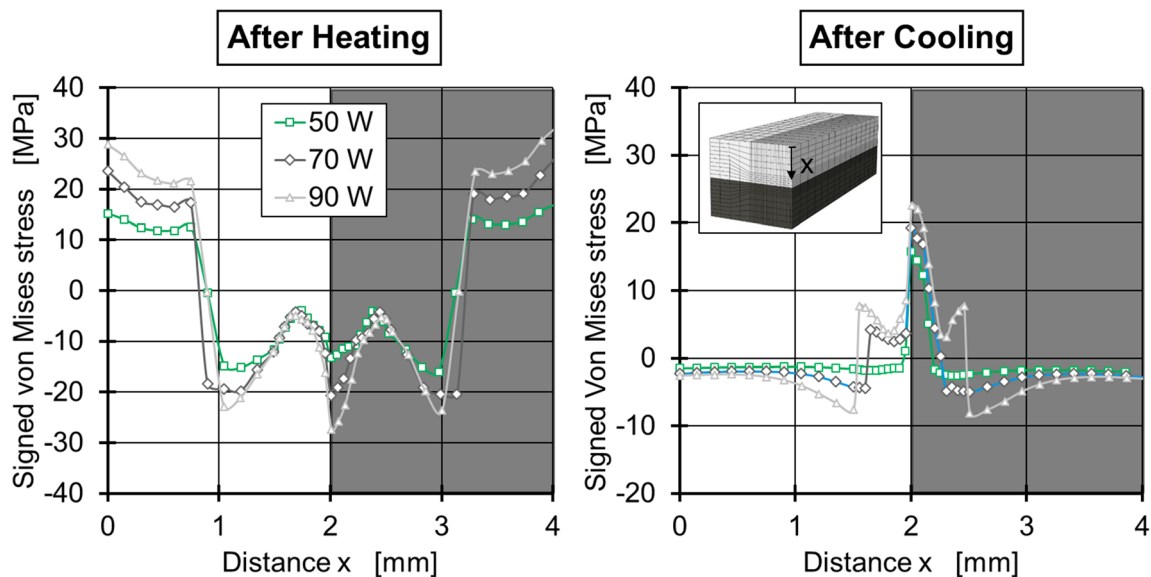


Fig. 13 Spatial signed von Mises stresses for the elastoplastic material model with laser powers of 50 W, 70 W, and 90 W after heating and cooling

process. Even if there is currently no method for the exact quantitative determination of internal stresses in the weld seam, the calculation results for the elastoplastic material model are classified as realistic.

Future work will combine the developed thermomechanical simulation with an interdiffusion model for strength prediction of welded components. The entire model is constructed for other materials (polycarbonate and polybutylene terephthalate) and validated by tensile tests with the welded specimens. Especially with highly scattering materials and resulting larger heat-affected zones, such as polybutylene terephthalate, it can be assumed that a stronger melt flow also occurred for the specimens under consideration. For such materials, it makes sense to combine the simulation with a flow simulation.

Funding information The depicted research has been funded by the Deutsche Forschungsgesellschaft (DFG) as part of the research project “Integrative calculation of the weld strength of plastics parts based on an interdiffusion model presented for laser transmission welding.” We would like to extend our gratitude to the DFG.

References

- Acherjee B, Kuar AS, Mitra S, Misra D (2012) Modeling of laser transmission contour welding process using FEA and DoE. *Opt Laser Technol* 44(5):1281–1289
- Apic S (2009) Untersuchung von Messmethoden zur Erfassung der Intensitätsverteilung beim Laserdurchstrahlschweißen. Institut für Kunststoffverarbeitung (IKV) in Industrie und Handwerk, RWTH Aachen, diploma thesis
- Becker F (2003) Einsatz des Laserdurchstrahlschweißens zum Fügen von Thermoplasten. Universität Paderborn, dissertation
- Beiss T (2016) Einführung, Technologie- und Branchenüberblick. *Umdruck zur Tagung Kunststoffe erfolgreich verbinden – Innovative Fügetechnologien für die Praxis*. Aachen
- Bonefeld D (2012) *Eigenstressungen, Spaltüberbrückung und Strahloszillation beim Laserdurchstrahlschweißen*. Universität Paderborn, dissertation
- Carlslaw HS, Jaeger JC (1959) *Conduction of heat in solids*. Oxford University Press, Oxford
- Chen M (2009) *Gap bridging in laser transmission welding of thermoplastics*. Queen’s University Ontario, dissertation
- Chen M, Zak G, Bates PJ (2013) Description of transmitted energy during laser transmission welding of polymers. *Weld World* 57(2): 171–178
- Coelho JP, Abreu MA, Pires MC (2000) High-speed laser welding of plastic films. *Opt Lasers Eng* 34(10):385–395
- De Gennes PG (1971) Reptation of a polymer chain in the presence of fixed obstacles. *J Chem* 55(1):572–579
- Fargas M, Wilke L, Meier O, Potente H (2007) Analysis of weld seam quality for laser transmission welding of thermoplastics based on fluid dynamical processes. Proceedings of the 65th Annual Technical Conference (ANTEC). Cincinnati (OH), USA
- Fiegler G (2007) *Ein Beitrag zum Prozessverständnis des Laserdurchstrahlschweißens von Kunststoffen anhand der Verfahrensvarianten Quasi-Simultan- und Simultanschweißen*. Universität Paderborn, dissertation
- Frick T (2007) *Untersuchung der prozessbestimmenden Strahl-Stoff-Wechselwirkungen beim Laserstrahlschweißen von Kunststoffen*. Friedrich-Alexander-Universität Erlangen-Nürnberg, dissertation
- Gere JM, Goodno BJ (2012) *Mechanics of materials*. Stamford, CENGAGE Learning
- Grewell D, Benatar A (2008) Semiempirical, squeeze flow, and intermolecular diffusion model. II. Model verification using laser microwelding. *Polym Eng Sci* 48(8):1542–1549
- Gross D, Hauger W, Schröder J, Wall W, Bonet J (2011) *Engineering mechanics 2 – mechanics of materials*. Springer-Verlag Berlin Heidelberg, Dordrecht, Heidelberg, London, New York
- Guevara-Morales A, Figueroa-Lopez U (2014) Residual stresses in injection molded products. *J Mater Sci* 43(13):4399–4415
- Gupta SK, Pal PK (2018) Analysis of through transmission laser welding of nylon6 by finite element simulation. *MPER* 9(4):56–69
- Hastenbergh CHV, Wildervanck PC, Leenen AJH, Schennink G (1992) The measurement of thermal stress distributions along the flow path in injection-molded flat plates. *Polym Eng Sci* 32(7):506–515

20. Hering E, Martin R, Stohrer M (2012) Physik für Ingenieure. Springer-Verlag GmbH Deutschland, Berlin
21. Ilie M, Kneip JC, Mattei S, Nichici A, Roze C, Girasole T (2007) Through-transmission laser welding of polymers – temperature field modeling and infrared investigation. *Infrared Phys Technol* 51(1):73–79
22. Jänecke M (2015) Leichtbau mit technischen Textilien. *Kunststoffe* 105(2):26–30
23. Jones I (2004) Laser welding of plastic components. *Assem Autom* 22(2):129–135
24. Kennish YC (2003) Development and modelling of a new laser welding process for polymers. University of Cambridge, dissertation
25. Kennish YC, Shercliff HR, McGrath GC (2002) Heat flow model for laser welding of polymers. Proceedings of the 60th Annual Technical Conference (ANTEC). San Francisco (CA), USA
26. Klein HM (2001) *Laserschweißen von Kunststoffen in der Mikrotechnik*. RWTH Aachen, dissertation
27. Korte J (1998) *Laserschweißen von Thermoplasten*. Universität-GH Paderborn, dissertation
28. Kreimeier S (2017) *Thermische Simulation des Laserdurchstrahlenschweißprozesses von teilkristallinen Thermoplasten*. RWTH Aachen, dissertation – ISBN: 978–3–95886-162-6
29. Kreimeier S, Hopmann C (2016) Modeling of the heating process during the laser transmission welding of thermoplastics and calculation of the resulting stress distribution. *Weld World* 60(4):777–791
30. Küsters K (2012) *Modellierung des thermo-mechanischen Langzeitverhaltens von Thermoplasten*. RWTH Aachen, dissertation – ISBN: 978–3–86130-513-2
31. Labeas GN, Moraitis GA, Katsiropoulos CV (2010) Optimization of laser transmission welding process for thermoplastic composite parts using thermo-mechanical simulation. *J Compos Mater* 44(1):113–130
32. Lakemeier P, Schoenppner V (2017) Simulation-based investigation of the temperature influence during laser transmission welding of thermoplastics. Proceedings of the 75th Annual Technical Conference (ANTEC). Anaheim (CA), USA
33. Mayboudi LS (2008) Heat transfer modelling and thermal imaging experiments in laser transmission welding of thermoplastics. Queen's University Ontario, dissertation
34. Mayboudi LS, Birk AM, Zak G, Bates PJ (2009) Infrared observations and finite element modeling of a laser transmission welding process. *J Laser Appl* 21(3):111–118
35. Messner RW (2004) Joining composite materials and structures: some thought-provoking possibilities. *J Thermoplast Compos Mater* 17(1):51–75
36. Michaeli W, Brandt M, Brinkmann M, Schmachtenberg E (2006) Simulation des nicht-linear viskoelastischen Werkstoffverhaltens von Kunststoffen mit dem 3D-Deformationsmodell. *Zeitschrift Kunststofftechnik - Journal of Plastics Technology* 2(5):1–24
37. N.N. (2014a) DVS-Richtlinie 2243 - Laserstrahlenschweißen thermoplastischer Kunststoffe. In: N.N. (Hrsg.): *Taschenbuch DVS-Merkblätter und Richtlinien*. Düsseldorf: DVS Media
38. N.N. (2014b) *Schneckenkonzepte beim Spritzgießen*. Technical Information, BASF SE, Ludwigshafen
39. N.N. (2016) Campus Datasheet Ultramid A3W. Datasheet, BASF SE, Ludwigshafen
40. N.N. (2018) *PlasticsEurope Annual Review 2012017–2018*. Annual Report, Plastics Europe AISBL, Brussels
41. Potente H (2004) *Fügen von Kunststoffen - Grundlagen, Verfahren, Anwendungen*. München, Wien, Carl Hanser Verlag
42. Potente H, Fiegler G (2004) Laser transmission welding of thermoplastics - modelling of flows and temperature profiles. Proceedings of the 62th Annual Technical Conference (ANTEC). Chicago (IL), USA
43. Potente H, Wilke L, Ridder H, Mahnken R, Shaben A (2008) Simulation of the residual stresses in the contour laser welding of thermoplastics. *Polym Eng Sci* 48:767–773
44. Rattunde L (2015) *Optimierung eines bestehenden Simulationsmodells zur Berechnung des Erwärmvorgangs beim Laserdurchstrahlenschweißprozess*. Institut für Kunststoffverarbeitung (IKV) in Industrie und Handwerk, RWTH Aachen, bachelor thesis
45. Reinl S, Rau A (2011) Laserkunststoffschiweißen in der industriellen Serienproduktion. *Laser Magazin* 28(2):17–21
46. Russek UA (2006) *Werkstoff-, Prozess- und Bauteiluntersuchungen zum Laserdurchstrahlenschweißen von Kunststoffen*. RWTH Aachen, dissertation
47. Schmidt A, Gaul L (2001) Bestimmung des komplexen Elastizitätsmoduls eines Polymers zur Identifikation eines viskoelastischen Stoffgesetzes mit fraktionalen Zeitableitungen. Proceedings of the DGZfP Jahrestagung. Berlin, Germany
48. Sparks JA (1997) Low cost technologies for aerospace applications. *Mircoprocess Mirco syst* 20(8):449–454
49. Stojek M, Stommel M, Korte W (1998) Finite-Elemente-Methode für die mechanische Auslegung von Kunststoff- und Elastomerbauteilen. Düsseldorf, Springer-VDI-Verlag
50. Wang C, Yan T, Liu H, Zhong H (2018) Temperature field and fluid field simulation of laser transmission welding polycarbonate. Proceedings of the 76th Annual Technical Conference (ANTEC). Orlando (FL), USA
51. Ward I (1983) *Mechanical properties of solid polymers*. Wiley, Chichester, New York, Brisbane, Toronto Singapore
52. Xu XF, Parkinson A, Bates PJ, Zak G (2015) Effect of part thickness, glass fiber and crystallinity on light scattering during laser transmission welding of thermoplastics. *Opt Laser Technol* 30(75):123–131
53. Zhou X, Lin H (2008) Sensitivity analysis. In: Boston, Shekhar, Shashi; Xiong, Hui (Hrsg.): *Encyclopedia of GIS*. Boston: Springer US
54. Zoubair T, Elhem G (2011) Numerical study of laser diode transmission welding of a polypropylene mini-tank: temperature field and residual stresses distribution. *Polym Test* 30(1):23–34

Publisher's note Springer Nature remains neutral with regard to jurisdictional claims in published maps and institutional affiliations.